

Dartmouth College

Dartmouth Digital Commons

Open Dartmouth: Peer-reviewed articles by
Dartmouth faculty

Faculty Work

1999

The Steep Spectrum Quasar PG1404+ 226 with ASCA, HST and ROSAT

Marie-Helene Ulrich
European Southern Observatory

Andrea Comastri
INAF - Osservatorio Astronomico di Bologna

Stefanie Komossa
Max Planck Institute for Extraterrestrial Physics

Phil Crane
Dartmouth College

Follow this and additional works at: <https://digitalcommons.dartmouth.edu/facoa>



Part of the [Astrophysics and Astronomy Commons](#)

Dartmouth Digital Commons Citation

Ulrich, Marie-Helene; Comastri, Andrea; Komossa, Stefanie; and Crane, Phil, "The Steep Spectrum Quasar PG1404+ 226 with ASCA, HST and ROSAT" (1999). *Open Dartmouth: Peer-reviewed articles by Dartmouth faculty*. 540.

<https://digitalcommons.dartmouth.edu/facoa/540>

This Article is brought to you for free and open access by the Faculty Work at Dartmouth Digital Commons. It has been accepted for inclusion in Open Dartmouth: Peer-reviewed articles by Dartmouth faculty by an authorized administrator of Dartmouth Digital Commons. For more information, please contact dartmouthdigitalcommons@groups.dartmouth.edu.

A&A manuscript no.
(will be inserted by hand later)

Your thesaurus codes are:
06 (03.11.1; 16.06.1; 19.06.1; 19.37.1; 19.53.1; 19.63.1)

ASTRONOMY
AND
ASTROPHYSICS

The Steep Spectrum Quasar PG1404+226 with ASCA, HST and ROSAT

M.-H. Ulrich¹, A. Comastri², S. Komossa³, and P. Crane^{1,4}

¹ European Southern Observatory, Karl-Schwarzschild-Strasse 2, D-85748 Garching, Germany

² Osservatorio Astronomico di Bologna, via Ranzani 1, I-40127 Bologna, Italy

³ Max-Planck-Institute für extraterrestrische Physik, Giessenbach Str., D-85748 Garching, Germany

⁴ Dept. of Physics and Astronomy, Wilder Laboratory, Dartmouth College, Hanover N.H. 03755, USA

Received xx, 1999; accepted xx, 1999

Abstract. We present and discuss our observations of the Narrow Line quasar PG1404+226 ($z_{em} = 0.098$) with ASCA and HST, and a re-analysis of our earlier observations with ROSAT. The soft X-ray spectrum is very steep and displays an absorption feature (edge or line at ~ 1.1 keV). We have applied a variety of models to the ASCA and ROSAT spectra without finding a completely satisfactory fit, and the identification of the edge remains uncertain. A satisfactory fit of the ASCA spectrum assuming that the edge is produced by highly ionized iron (using the code `absori` in XSPEC) is obtained with an overabundance of iron by a factor ≥ 25 compared to solar, a suggestion supported by the extremely high equivalent width of the Fe K α line at 6.4 keV. A warm absorber model (based on Cloudy) fitting the absorption feature with NeVII-NeX edges and assuming a peculiar oxygen/neon abundance ratio is consistent with the ROSAT data but not the ASCA data. Finally, it is also possible that the observed edge is caused by a OVIII or OVII edge or line, blueshifted by $z_{abs} = 0.2$ to 0.5 depending on the specific identification, as has been suggested previously for 2 other Narrow Line quasars, but there are no other features in the UV and X-ray spectra in support of this suggestion.

Two systems of UV absorption lines, one nearly at rest in the source frame, the other blueshifted by ~ 1900 km s⁻¹ are identified in the HST/FOS spectra. Photoionization models indicate that the UV absorption and the ~ 1 keV absorption are probably caused by absorbers with different physical conditions. PG1404+226 is one more case of AGN where both UV and X-ray absorption features are detected, thereby increasing further the significance of the previously noted statistical association of the two types of absorbers.

Key words: galaxies: active – galaxies:Seyfert X rays: galaxies – UV: quasars – PG 1404+226

Send offprint requests to: M.-H. Ulrich

1. Introduction

Narrow Line Active Galactic Nuclei form a distinct class of AGN on the basis of the properties of their optical/UV spectrum: full width at half maximum (FWHM) of the hydrogen lines and other lines in the range 500-2000 km s⁻¹, intense high ionization lines, and intense FeII multiplets (Osterbrock & Pogge, 1985; Shuder & Osterbrock, 1981). The weakest of these AGN, the Narrow Line Seyfert 1 (NLS1), and the somewhat brighter AGN with absolute optical luminosity above but close to the lowest limit for quasars of $M_v = -23.4$ have been extensively studied in the X-ray range (e.g. Laor, Fiore, Elvis et al., 1994; Boller, Brandt & Fink, 1996; Laor et al., 1997). Among all AGN, the Narrow Lines AGN tend to have the steepest soft X-ray spectra (ROSAT), and some of them show fast, large amplitude soft X-ray variability with occasionally giant outbursts (e.g. Grupe 1996 and references therein; Boller et al 1996). In the harder 2-10 keV band a comparative study of a large sample of NLS1 and broad line Seyfert 1s revealed that the 2-10 keV ASCA spectral slopes of NLS1 are significantly steeper than those of broad line AGN (Brandt, Mathur & Elvis 1997).

Recent BeppoSAX observations of a selected sample of bright NLS1 (Comastri, Fiore, Guainazzi et al. 1998; Comastri, Brandt, Leighly et al. 1998) over the broad 0.1-10 keV range indicate that a two component model provides an adequate description of the X-ray continuum. The relative strengths and slopes of the two components are different from those of broad line Seyfert 1s. The NLS1 are characterized by a stronger soft excess and, in general, have a steeper medium energy X-ray power law with respect to normal Seyfert 1s, but in PG 1404+226 the medium energy spectral index is not very different from that of classical Seyfert 1s while its soft excess is strong,

very steep and rapidly variable like in other NLS1. The spectral behaviour of NLS1 suggests that the soft X-ray flux cannot be due only to disk reprocessing unless there is highly anisotropic emission. In the framework of the thermal models for the X-ray emission in Seyfert 1s (Haardt & Maraschi 1993) a strong soft component could lead to a strong Compton cooling of the hot corona electrons and to a steep hard tail. This hypothesis is also supported by the similarities between NLS1 spectra and those of Galactic black hole candidates in their high states first suggested by Pounds, Done and Osborne (1995) and Czerny et al. (1996).

The high states of Galactic black hole candidates are thought to be triggered by increases in the accretion rate possibly reaching values close to the Eddington limit. In this case the disk surface is expected to be highly ionized, in good agreement with the observation of a H-like Fe edge in TonS180 (Comastri et al. 1998a). It should also be noted that a high L/L_{Edd} ratio would also be consistent with the narrowness of the optical lines in NLS1 if the optical line producing region is virialized as suggested by Laor et al. (1997)

The quasar PG 1404+226 ($z = 0.098$, $V = 15$) is one of the brightest members of the class of Narrow Line AGN. The optical spectrum of PG 1404+226 displays the characteristics of NLS1 with FWHM ($H\beta$) $\simeq 830 \text{ km s}^{-1}$ and strong Fe II emission (Boroson & Green 1992). The observations with the ROSAT PSPC (~ 0.1 – 2.0 keV) showed a very steep spectrum ($\Gamma \sim 3$) with rapid flux (a factor 2 in 10 hours) and spectral variability typical of NLS1 in the X-ray range, and revealed a complex absorption feature around 0.8–1.0 keV (Ulrich & Molendi 1996, thereafter UM96). Time resolved spectral analysis showed the data to be consistent with a shift of the absorption feature to higher energy when the source brightens (UM96).

We have obtained a 40 ks ASCA observation of PG 1404+226 in order to investigate the X-ray spectrum over a larger energy range and at higher energy resolution than was possible with ROSAT. At the time of the ASCA observations the absorption feature was around 1 keV, at an energy definitely higher than that of the OVII and OVIII edges at 0.74 and 0.87 keV commonly seen in ASCA and ROSAT spectra of AGN (e.g. Reynolds 1997). Preliminary results can be found in Comastri, Molendi & Ulrich (1997, hereafter CMU97). The ASCA and ROSAT data have been fit separately since they have not been obtained at the same epoch. The challenge presented by PG 1404+226 is the identification of the absorption at $\sim 1.1 \text{ keV}$. Brandt et al (1994) found a similar feature at 1.15 keV in Ark 564 and considered several interpretations: Neon edge, iron L edges, and outflowing material which would raise the energy edge of OVIII (0.870 keV) to the observed energy. They find none of them to be satisfactory: neon edge because there is only a narrow range of ionization parameter where it would be stronger than the OVIII edge; the iron L edges would produce absorp-

tion at other somewhat higher energy (1.358 keV); and the outflow seems unlikely because the source of its kinetic energy is unclear. Otani et al (1996) found a feature at $\sim 1 \text{ keV}$ in IRAS 13224-3809 for which they suggest an interpretation in terms of outflow, or alternatively and considering that the the X-ray flux of IRAS 13224-3809 varied by a factor 50 in two days “the ionization state of the medium is far from equilibrium due to the violent variability”. Krolik & Kriss (1995) drew attention to the fact that “because the ionization timescales of some ions may be as long as the variability timescales in AGNs, the ionic abundances indicated by the transmission spectra may not be well described by ionization equilibrium”. This point has recently been re-investigated by Nicastro et al. (1999a) who pointed out also that (i) Recombination times can be longer than photoionization times resulting in gaseous absorbers which are over-ionized with respect to the equilibrium ionization state and (ii) Collisional ionization could be of comparable importance to photoionization.

Hayashida (1997) found an edge near 1 keV in H0707-495 for which he also suggests an identification with a bluishifted OVIII absorption edge. For PG 1404+226, CMU97 suggested an overabundance of iron, an interpretation which has the advantage to link the origin of the 1 keV absorption to the intense FeII lines present in the optical/UV of this quasar and also of IRAS 13224-3809 and Ark 564. The interpretation where the absorption near $\sim 1 \text{ keV}$ originates in hot gas outflowing at velocities in the range 0.2 - 0.5c has also been proposed by Leighly et al (1997).

This paper presents an analysis of the ASCA observations, a re-analysis of the ROSAT spectra with our warm absorber (WA) models calculated with CLOUDY (Ferland 1993), and an analysis of HST spectra which we have obtained in order to search for UV absorption/emission lines.

2. Re-analysis of the ROSAT data

The data reduction was carried out in a standard manner and like in UM96 the data were split into “high-state” and “low-state” depending on count rate. The analysis was performed with our warm absorber models based on CLOUDY.

The warm absorber is assumed to be of constant density, of solar abundances (if not mentioned otherwise), and to be illuminated by the continuum of the central point-like energy source. The spectral energy distribution from the radio to the gamma-ray region consists of piecewise powerlaws with, in particular, an energy index in the EUV, $\alpha_{uv,x}$, of 1.4 and an X-ray photon index Γ_x of 1.9. A black-body-like soft excess is added in some models. The column density N_{WA} of the warm material (i.e. the total column density in Hydrogen) and the ionization parameter U are determined from X-ray spectral fits (Table 1). U

Table 1. X-ray spectral fits to the high-state (HS) and low-state (LS) *ROSAT* data of PG 1404. Γ_x was fixed to 1.9. Errors in U , N_{WA} are about a factor 2–3.

state	$\log U$	$\log N_{\text{WA}}$	χ^2_{red}	model
HS/LS			4.1/2.0	single PL
HS/LS	1.0/0.7	23.7/23.4	2.5/0.9	standard warm absorber
HS/LS	1.0/0.7	23.8/23.5	2.2/0.9	emission+reflection added
HS/LS	0.7/0.3	23.3/22.9	1.3/0.9	Ne = 4×solar abundance
HS/LS	0.6/0.4	23.1/23.1 ⁽¹⁾	1.2/1.0	additional 0.1 keV soft excess ⁽²⁾

⁽¹⁾ fixed to value derived for HS; ⁽²⁾ abundances reset to solar

is a measure of the number rate of ionizing photons above the Lyman limit and is defined by

$$U = Q / (4\pi r^2 n_{\text{H}} c) \quad (1)$$

where Q is the number rate of incident photons above the Lyman limit, r is the distance between central source and absorber, c is the speed of light, and n_{H} is the hydrogen density (fixed to $10^{9.5} \text{ cm}^{-3}$ unless noted otherwise). As detailed below, several models give acceptable fits to the low-state spectrum but none gives a really good fit to the high-state spectrum (which has a higher signal/noise ratio).

2.1. Results with a simple power law

A simple power law plus cold absorption gives a very poor fit. The cold absorbing column generally tends to slightly underpredict the Galactic value. This may reflect some low energy calibration uncertainties, or the presence of an additional spectral component in the form of a very soft excess. Adding a soft excess parameterized as a black body which contributes only at very low energies (e.g. in NGC4051, Komossa & Fink 1997; Ton S180, Fink et al. 1997) improves the fit which, however, remains unsatisfactory.

2.2. Results of the Spectral fits with Warm absorber models

We have examined a family of models (labelled a,b,..e; Table 1) which include a warm absorber plus a power law component with a photon index Γ_x fixed at 1.9.

2.2.1. Model a and b: solar abundances

Model a: The inclusion of a ‘standard’ warm absorber model clearly improves the fit but does not yield an acceptable χ^2 , with systematic residuals remaining near 1 keV. The reason is that, even for very high ionization parameters, the model has a strong oxygen absorption at 0.87 keV, even stronger than the neon absorptions (NeVII at ≈ 1.1 keV and NeX at ≈ 1.36 keV). This is exacerbated at high-state because the high-state data require absorption around the location of the neon edges to dominate.

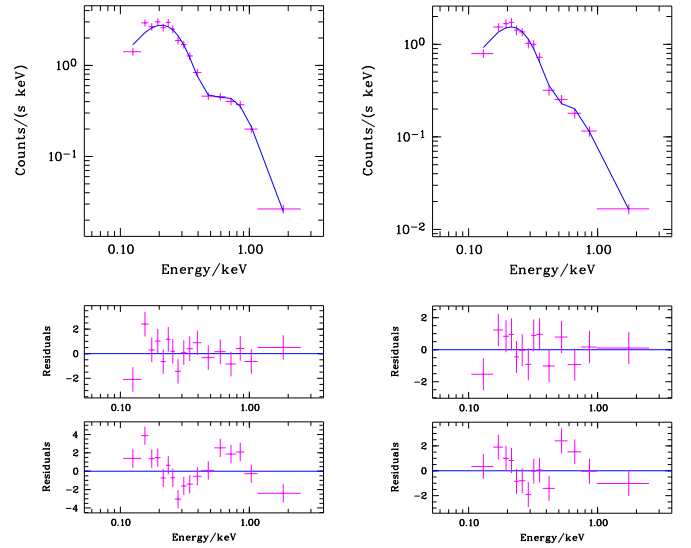


Fig. 1. X-ray spectrum (crosses) for fit of model (e) (continuous line) to the *ROSAT* high state (left) and low state (right). Immediately underneath are the corresponding residuals for this model. The bottom panels are the residuals for a single power law fit of the *ROSAT* high state (left) and low state (right).

(The same results hold for a steeper underlying power-law.)

Model b: The addition of the emission and reflection components of the warm material, calculated for a covering factor of 0.5 results in a slightly improved fit, but the high-state data are still not well matched.

2.2.2. Model c: non-solar abundances

One way to make the neon absorption dominate over the oxygen absorption is to introduce deviations from solar abundances, with overabundant neon, or underabundant oxygen.

Several deviation factors were studied between an oxygen abundance of up to $\text{O} = 0.2 \times \text{solar}$ and a neon abundance of $\text{Ne} = 4 \times \text{solar}$. These models strongly improve the quality of the fit and the values of χ^2 reach acceptable values (for the *ROSAT* spectra). The best fit has an overabundance of neon of ~ 4 times the solar value.

We note that while non solar abundances have been reported in a number of AGN/quasars (e.g. Hamann & Ferland 1993, Netzer 1997) the ratio O/Ne is expected to remain close to its solar value in all known astrophysical situations (On the other hand, Netzer occasionally depletes *oxygen only* in his photoionisation models, e.g. Marshall et al. 1993). In any event, the model with overabundance of neon is not compatible with the ASCA data (Section 3.2.2).

2.2.3. Model d and e: additional soft excess (and solar abundances)

Model d: Motivated by the ASCA evidence for the presence of a soft excess, a sequence of models was calculated with an additional hot BB component of $kT = 0.1$ keV. This component was included in the ionizing spectral energy distribution that illuminates the warm absorber, i.e. the change in ionization structure of the warm material was self-consistently calculated. A successful description of both, high- and low-state data is possible with solar abundances. Note that two-component models *without edge*, specifically, power law + blackbody and power law + bremsstrahlung were found to provide satisfactory fits of the ROSAT data at low state. For the high state data the power law + blackbody model gives $\chi^2 = 67/20$ (UM96).

Model e: U and N_{WA} have above been treated as free parameters, and the fits tend to give slightly different column densities in low- and high-state data, whereas this quantity is not expected to vary within short time-scales (10 hours or less). We therefore have searched for the best fit model (model e) to the high- and low-state data in which the column density is identical in both states and only the ionization parameter U and the strength of the BB component are allowed to vary between states. We find a successful model with $\log(N_{WA}) = 23.1$, $\log(U_{high}) = 0.6$, $\log(U_{low}) = 0.4$, and a contribution of the blackbody to the ionization parameter of $\log(U_{BB}) = \log(U_{PL}) - 0.9$ in the high-state data and $\log(U_{BB}) = \log(U_{PL}) - 1.5$ in the low-state data (Fig. 1; U_{BB} and U_{PL} are the ionization parameters related to the blackbody component, and powerlaw component, respectively. U is a measure of the number rate of ionizing photons above the Lyman limit. See Eqn. (1) for the definition of U).

3. ASCA Observations and Spectral Analysis

3.1. Observations

PG 1404+226 was observed by ASCA (Tanaka, Inoue & Holt 1994) July 13-14, 1994 with the Gas Imaging Spectrometers (GIS2/GIS3) for a total effective exposure time of 35000 s, and with the Solid-state Imaging Spectrometers (SIS0/SIS1) for about 29000 s.

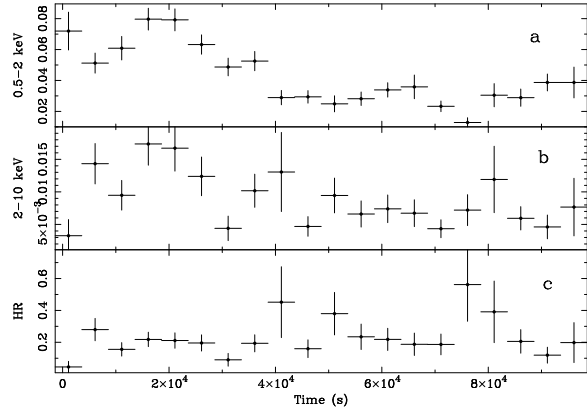


Fig. 2. Intensity and hardness ratio light curves of PG 1404+226 during the ASCA observations (for ROSAT observations see fig 3 in UM96). Panel a) SIS0 light curve (counts/s) in the 0.5-2 keV energy range. Panel b) SIS0 light curve (counts/s) in the 2-10 keV energy range. Panel c) Hardness ratio (0.5-2/2-10 keV) light curve.

The SIS was operating in 1-CCD mode and all the data were collected in Faint mode. Standard criteria for the good selection intervals have been applied (i.e. Cut-off rigidity > 7 for GIS and > 6 for SIS, minimum elevation angle from the earth > 5 degrees and minimum bright earth angle > 25 degrees for SIS) as well as DFE and echo corrections. The background subtracted count rates for PG 1404+226 are 0.049, 0.038, 0.014, 0.017 c/s in S0, S1, S2, S3 respectively.

Large flux variations have been detected. In panels a and b of Fig. 2 we show the soft (0.5–2.0) and hard (2.0–10 keV) SIS0 light curves. The SIS0 light curve in the soft band (Fig. 2a) shows a factor ~ 4 of amplitude variability with a doubling timescale of ~ 8000 s. The variability pattern in the two bands is well correlated suggesting that the hard and soft fluxes varied in the same way.

A detailed spectral resolved temporal analysis is hampered by the low counting statistics especially at high (> 2 keV) energies. In order to have some indications on the spectral variability we have performed a hardness ratio analysis for the high (first part of the observation) and the low (second part of the observation) state shown in Figure 2. The hardness ratio (Fig. 2c) has been defined as $HR = (H-S)/(H+S)$ where H and S are the counts in the 2–10 and 0.5–2 keV bands respectively. The results for the high and low state are $HR_{Highstate} = -0.79 \pm 0.06$ and $HR_{Lowstate} = -0.75 \pm 0.04$ suggesting that the spectrum is rather soft in both states. The 2–10 keV flux is rather low and as a consequence both the 2-10 keV light curve and the hardness ratio light curve are noisy with no clear evidence of spectral variability in contrast to the spectral change during the ROSAT observations.

Table 2. ASCA spectral analysis

Model	Γ or kT ⁽¹⁾	Γ ⁽²⁾	E_{edge}/E_{cut} ⁽³⁾	τ/E_{fold} ⁽⁴⁾	χ^2/dof
PL	3.48 ± 0.10	438.3/146
PL+PL	3.95 ± 0.15	$0.85^{+0.21}_{-0.31}$	291.5/144
BR+PL	246^{+17}_{-15}	1.48 ± 0.18	235.7/144
BB+PL	126 ± 4	$1.62^{+0.15}_{-0.11}$	196.0/144
BB+PL+EDGE	138 ± 6	$1.92^{+0.19}_{-0.16}$	1.07 ± 0.03	0.88 ± 0.26	158.6/142
CUTBB+PL	139 ± 8	$1.91^{+0.10}_{-0.15}$	$0.94^{+0.05}_{-0.07}$	51^{+96}_{-45}	159.5/142

⁽¹⁾ Power law slope or thermal model temperature (in eV) for the soft component;

⁽²⁾ Power law photon index for the hard component;

⁽³⁾ Edge energy / Exponential cutoff energy (in keV);

⁽⁴⁾ Edge optical depth / e-folding energy of the exponential cutoff in eV

The spectral analysis has thus been performed on the spectrum accumulated over the entire duration of the ASCA observation. The average luminosity is comparable with the ROSAT low state but the absorption feature is at high energy as during the ROSAT high state.

3.2. Spectral Analysis

GIS and SIS spectra were binned with more than 20 counts/bin in the 0.7–10 keV and 0.5–10 keV energy ranges respectively. Since the spectral parameters obtained by fitting the four detectors separately were all consistent within the errors, the data were fitted simultaneously to the same model.

Given the very low Galactic column density toward PG 1404+226 ($2 \times 10^{20} \text{ cm}^{-2}$; Elvis, Lockman & Wilkes 1989) and the low sensitivity of ASCA detectors for small column densities, all the spectral fits have been performed with $N_H \equiv N_{HGal}$. This choice is also corroborated by the ROSAT results (UM96).

A single power law model clearly does not provide an acceptable fit (Table 2) The power law fits reported in Table 2 suggest that at least two components are required to fit the overall spectrum. We note that the slope of the hard power law, which could not have been detected by ROSAT, is consistent with the average quasar slope (Comastri et al. 1992) while the slope below 2 keV is consistent with the UM96 findings.

In order to model the broad band (0.4–10 keV) spectrum we tried 4 types of double component fits (See Table 2 for details): a double power law, bremsstrahlung plus power law, blackbody plus power law, and cut-off blackbody plus power law (the cut-off is of the form $\exp[-(E - E_c)/E_f]$ for energies larger than the cutoff energy $E_c \sim 0.94 \text{ keV}$. The depth of the cut-off is related to E_f , a small value corresponding to a very steep decline of the intensity; here $E_f \sim 0.05 \text{ keV}$).

The first two models give unacceptable fits. The only two acceptable descriptions of the data are the cut-off blackbody plus power law (with a cut-off at 0.94 keV) and

the blackbody plus power law plus absorption edge model around 1 keV. The addition of the absorption edge to the simple blackbody plus power law model produces an improvement in the fit which is significant at $> 99.99\%$ (F-test) and the residuals are featureless in agreement with the results of Leighly et al (1997).

3.2.1. Is iron overabundant?

As absorption edges are the signature of warm absorbing material, we fit the warm absorber model available in XSPEC 9.0 (the model is ‘absori’ and the iron abundance is a free parameter; it was developed by P. Magdziarz & A. Zdziarski following Done et al 1992 and Zdziarski, Ghisellini, George et al. 1990). Given the relatively large numbers of free parameters in this model we have fixed the temperature of the warm material at $T = 10^5 \text{ K}$ (see for example Reynolds & Fabian 1995; the fits are not sensitive to the temperature, a change of $\log T$ from 4.5 to 6 would make no significant difference) and the iron abundance at the solar value. In addition we have considered only the 0.5–3.0 keV energy range in order to avoid contamination from the high energy component. We were not able to find any acceptable solution as can be judged from figure 3. Leaving the iron abundance free to vary the improvement is significant at $> 99.9\%$ (F-test) and the residuals featureless (Fig 4). The resulting parameters are: $\xi = 3000^{+500}_{-1000} \text{ erg cm s}^{-1}$, $N_H = 8^{+9}_{-1} \times 10^{20} \text{ cm}^{-2}$, Iron abundance > 25 solar and power law photon slope of 3.55 ± 0.12 . (All the quoted errors are at 90% confidence for one interesting parameter, $\chi^2_{min} + 2.7$).

The shape of residuals around 6–7 keV are suggestive of iron line emission (Fig 5). With the addition of a narrow line the improvement in the fit is, however, significant only at the 2σ level. The derived parameters are $E_{K\alpha} = 6.5 \pm 0.3 \text{ keV}$ and $EW = 1290 \pm 680 \text{ eV}$.

It is interesting to note that the huge equivalent width of the iron line is qualitatively consistent (see figure 3 in Reynolds, Fabian & Inoue, 1995) with the supersolar iron abundance found by fitting the data with the warm absorber model.

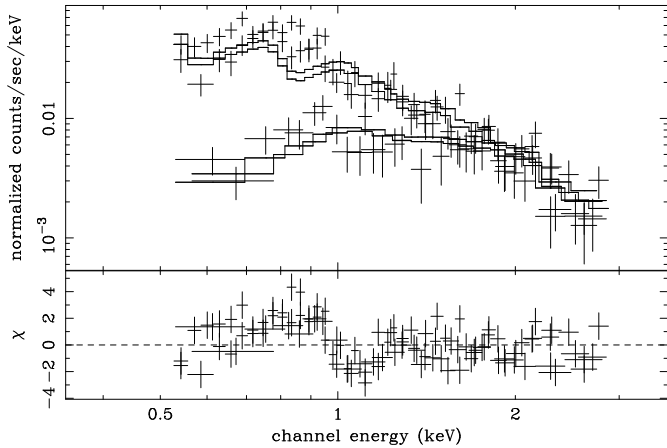


Fig. 3. The 0.5–3 keV ASCA spectrum fitted with a power law plus a warm absorber model with the iron abundances fixed at the solar value. The four ASCA detectors are fitted simultaneously leaving the relative normalizations free to vary.

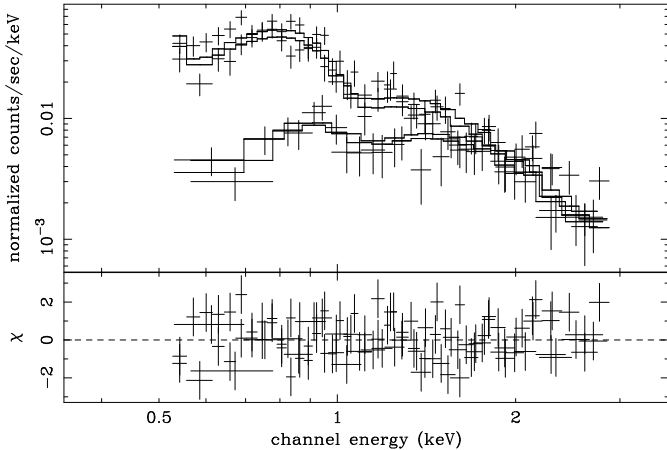


Fig. 4. The 0.5–3 keV ASCA spectrum fitted with a power law plus a warm absorber with super-solar iron abundances. The four ASCA detectors are fitted simultaneously leaving the relative normalizations free to vary.

3.2.2. Non-solar abundances of Neon or Oxygen?

We have also attempted to fit some warm absorber models (cloudy based, and with blackbody + power law continuum) to the ASCA spectrum and have found no satisfactory fit - the reason being that the edge-like feature at 1 keV is too deep and too narrow for these models.

3.2.3. Resonant Absorption ?

It has been recently shown that the spectra emerging from ionized gas are strongly modified by resonant absorption if the dispersion velocity in the gas is of the order of 100 km s⁻¹ or greater (Nicastro, Fiore, Matt 1999b). The X-ray warm absorber features are also strongly dependent from the shape of the ionizing continuum. For soft X-ray

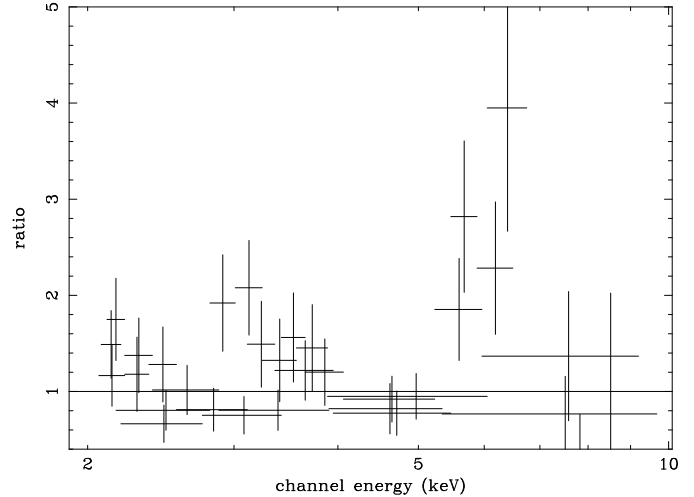


Fig. 5. The residuals of a power law fit to the ASCA data in the 2–10 keV energy range. The two GIS and the two SIS have been added. A line-like excess is evident around 6 keV (observed frame).

spectra as steep as the one observed for PG 1404+226 several resonance absorption lines from Fe L, Mg, Si and S are predicted between 1 and 2 keV. Such blend of lines would appear as negative residuals in low resolution ASCA spectra. The ~ 1 keV absorption feature of PG 1404+226 could be, at least in part, accounted for by resonant absorption. Signatures of this process have been looked for in the HST UV spectrum (see below).

3.2.4. Is the ~ 1 keV absorption the blueshifted OVIII edge?

Finally, we have also considered the possibility that the absorption at 1.07 keV is the blueshifted OVIII edge whose rest frame energy is 0.87 keV.

We have calculated the optical depth expected for the Neon edges at rest energies 1.1 and 1.36 keV which would be blueshifted to 1.29 and 1.55 keV respectively. For the 1.1 keV line the instrumental upper limit on τ is 0.14 (90% confidence level) and is 0.27 for the 1.36 keV edge.

We note that with a ‘standard’ warm absorber in relativistic outflow the OVIII edge is never the “only” edge in the spectrum. If the absorber is lowly ionized, there is OVII co-existing and if it is very highly ionized, OVII becomes negligible, but one cannot avoid having some Neon absorption. Although the exact ratios of the optical depths τ depend on the input parameters, we thought it would be useful to check whether we could detect any other edge, or check how strict the upper limits are. We take NGC 4051 as basis for comparison. In NGC 4051, the absorber is rather highly ionized, with OVIII being the strongest edge with $\tau = 1.1 \pm 0.4$, then NeX with $\tau = 0.8 \pm 0.4$. The OVII edge is weaker with $\tau = 0.35$; Komossa & Fink, 1997. Using the ratio τ_{OVIII}/τ_{NeX} as typical for the relative

depths in a highly ionized absorber, we can conclude that our non-detection of edges other than the one near 1.1 keV in PG1404+226 is still consistent with a standard warm absorber i.e. our upper limits on τ are not strict enough to rule out a warm absorber in relativistic outflow.

4. HST and IUE Observations

4.1. Observations

Four spectra were taken in February 1996 with HST/FOS and gratings G130, G190H, G270 and G400 with integration times 2300, 530, 120 and 120 seconds respectively. The total observed wavelength range covered is 1087 - 4773 Å with a nominal resolution of 1300 (Fig.6). The spectra were taken through the 0.86 arcsec diameter aperture. Standard reduction procedures were performed. The wavelength scale of the spectrum taken with G190H was shifted by +1.5 Å, to be consistent with the other spectra.

PG 1404+226 was observed with IUE on July 1994, 2 days after the ROSAT observations. The spectrum, SWP 51419, has a total integration time of 315 minutes (accumulated in 12 parts), and was taken through the large aperture and at low dispersion. Compared with the HST spectra taken 18 months later the continuum flux in July 1994 is ≈ 1.3 times brighter in the common observed wavelength range 1265 to 1400Å but the Ly α line kept the same intensity. The modest S/N and spectral resolution of the IUE spectrum would prevent the detection of the absorption lines seen in the HST spectra. No change in the emission/absorption profile of Ly α (Fig.7) can be detected by comparing the IUE spectrum and the FOS-G130 spectrum rebinned at 2Å.

4.2. Continuum and emission lines

Table 3 lists the emission line intensities ($H_0 = 50 \text{ km s}^{-1} \text{ Mpc}^{-1}$, $q_0 = 0$, distance = 617 Mpc). We note the presence of some weak emission lines: (1) an unidentified line at 1175Å (rest wavelength 1070Å) noticed in a few other quasar spectra (Laor et al 1995; Hamann et al 1997) (2) a line at 1290 Å which we identify with CIII*1175.7.

This line is seen in HST spectra of IZw1 and Laor et al (1997) suggest that it is produced by resonance scattering of continuum photons by CIII* ions, a mechanism which requires large velocity gradients ($\approx 1000 \text{ km s}^{-1}$) within each emitting cloud of the BLR.

4.3. The two systems of absorption lines and their likely origin

We identify two absorption systems in the HST spectra which, in the source frame, are separated by $\sim 1920 \text{ km s}^{-1}$. In the ‘blue’ system the absorption lines appear in the blue flank of the Ly α and CIV emission lines at 800 km s^{-1} from the peak. In the ‘red’ system the absorption

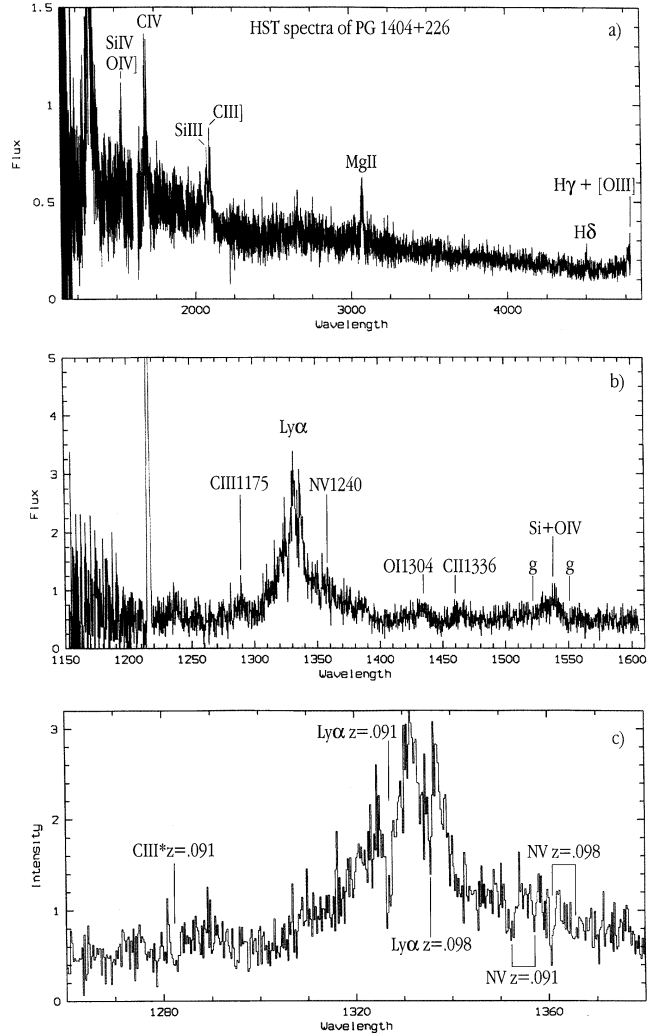


Fig. 6. HST spectra of PG1404+226: a) in the observed range 1150-4773 Å b) the FOS/G130 spectrum and the emission lines identification c) the Ly α and NV absorption lines identification.

lines appear on the red flank of the emission lines at 1100 km s^{-1} from the peak. It is known that in radio quiet AGN/Quasars, the high ionization lines such as CIV are blueshifted with respect to the systemic velocity by a few hundred to a few thousand km s^{-1} (e.g. van Groningen 1987, Corbin 1995, Sulentic et al. 1995) this blueshift being generally interpreted as evidence for a wind outflowing from the face of the accretion disk turned towards us. On this basis, we argue that the red absorption system is close to zero velocity in the source frame while the blue system originates from material which has an outflow velocity of $\sim 1900 \text{ km s}^{-1}$ (towards us with respect to the quasar).

Several factors hamper the measurement of the absorption lines: modest S/N, limited resolution of FOS and uncertainties affecting the profile of the emission lines. The absorption lines were measured assuming a plausible re-

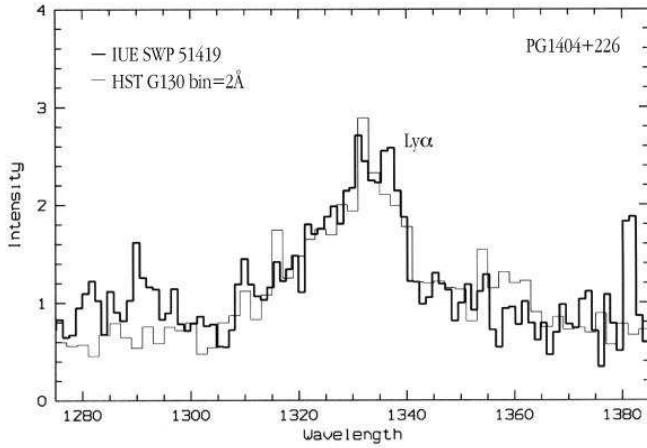


Fig. 7. The Ly α line in the IUE spectrum of 16 July 1994 (thick line) and the HST spectrum of February 1996 rebinned with 2 Å bins (thin line).

Table 3. Emission Lines Intensity in the HST Spectra of PG 1404+226

Identification	λ_{meas}	Observed Flux in 10^{-14} ergs s $^{-1}$ cm $^{-2}$	Intrinsic Flux in 10^{41} ergs s $^{-1}$
OVI 1033.83	1135.15	t	t
HeII 1085.15	1191.5	1.2	5.4
CIII 1175.70	1290.0	1.2	5.4
Ly α 1215.67	1334.8	54	245
NV 1240.15	1361.7	–	–
OI 1304.46	1432.25	2.5	11.3
CII 1334.53	1465.0	1.2	5.4
SiIV 1396.76	1533.6	3.5	15.9
NIV] 1486.50	1632.2	–	–
CIV 1549.05	1700.85	11.5	52.2
HeII 1640.50	1801.3	–	–
SiIII] 1892.03	2074.75	SiIII]+CIII] 9.9	45.0
CIII] 1908.73	2093.9	–	–
MgII 2795.53	3069.0	4.5	20.4
MgII 2802.70	3078.1	–	–
H δ	4945.4	1.0	4.5
H γ +[OIII]	–	1.3	5.9

Footnote: $H_0 = 50 \text{ km s}^{-1} \text{ Mpc}^{-1}$, $q_0 = 0$

construction of the top of the emission lines. Still it is not possible to obtain sufficiently accurate Ly α absorption profile, and NV and CIV doublet ratios to ascertain whether these lines are optically thin or thick and to estimate the covering factor (some of the galactic lines do not reach zero either). Higher spectral resolution is needed to elucidate these important points. With this caveat, the measures are given in Table 4.

Table 4. Absorption Lines in the HST Spectra of PG 1404+226

λ (Å) meas.	Identification	z meas.	EW (Å) meas.
Galactic lines:			
1206.5	SiIII 1206.50		0.6
1259.8	SiII 1260.42		t ⁽¹⁾
2795.5	MgII 2795.53		0.8
2802.5	MgII 2802.70		0.95
2851.7	MgI 2852.13		t
Abs. System at $z=0.091$			
1282.5	CIII*1175.70	0.09084	0.6
1327.0	Ly α 1215.57	0.091579	1.2 ⁽²⁾
1352.4	NV 1238.81	0.091700	0.6
1356.3	NV 1242.79	0.091330	0.2
1521.2	SiIV 1393.76	0.09144	0.3
	SiIV 1402.77		– ⁽¹⁾
1688.5	CIV 1548.19	0.090630	1.1 ⁽²⁾
1691.5	CIV 1550.76	0.090750	0.8
Abs. System at $z=0.098$			
1334.60	Ly α 1215.57	0.097830	0.95 ⁽³⁾
1360.65	NV 1238.81	0.098360	0.4
1365.45	NV 1242.79	0.098690	0.25
–	SiIV 1393.76		–
1538.5	SiIV 1402.77	0.0967	t
1699.1	CIV 1548.19	0.097480	0.55
–	CIV 1550.76		–
2860.0	FeII2599.4 ?	0.10	0.7

Footnotes:

⁽¹⁾ t trace; - not detected

⁽²⁾ EW of the lines of Ly α and CIV are measured after reconstruction of the emission lines top.

⁽³⁾ Galactic CIII1334.5,1335.6 likely contributor to Ly α at $z=0.098$

4.4. The CIII*1175 absorption line

Particularly interesting is the absorption line at 1282.5 Å (FWHM of 2 Å and EW of ≈ 0.7 Å), which could be CIII*1175 in the $z = 0.091$ system. The agreement in redshift is good. This line is present in the IUE and HUT spectra of NGC 4151 (Bromage et al 1985, Kriss et al 1992). Bromage et al (1985) argue that absorption by the excited metastable level of CIII*1175 and its strength relative to CIV 1549 require this level to be collisionally populated in a high density medium with $N_e = 10^{10} \text{ cm}^{-3}$. In NGC 4151, the EW of CIII*1175 is between 0.7 and 1.0 times the EW of CIV1548,1550 while in PG1404+226, it

is between 0.35 and 0.5 the EW of CIV1548,1550. Note that an appealing alternative for the identification of this line is the *CIV doublet blueshifted* by 0.3 with respect to PG1404+226. The line width, only $\approx 2 \text{ \AA}$, however, argues against this interpretation. There is no other candidate for highly blueshifted absorption lines in the spectrum.

4.5. Origin of the UV absorption systems

The $z = 0.098$ system is consistent with being produced in the halo of the host galaxy or of a nearby companion but could also be intrinsic to the nucleus. As for the $z = 0.091$ system the probable presence (which needs verification) of the CIII*1176 line suggests that the system is intrinsic to the quasar and forms in an outflowing wind with a velocity of 1900 km s^{-1} .

5. Do the UV and X-ray absorption lines come from the same absorber?

5.1. UV absorption lines from the Warm Absorber

(a) The EW of the UV absorption lines expected from the Warm Absorber have been calculated for the statistically acceptable models of the ROSAT data. They are given in Table 5, separately for low- and high-state as a measure of the uncertainty arising from the continuum variability (non simultaneous UV and X-observations, non- equilibrium of the gas, etc. see Section 1 and Nicastro et al. 1999a).

We find that the CIV1550 and NV 1240 absorption lines are weak at low state, and negligible at high state (because C and N are highly ionized). There is always some absorption by hydrogen due to the large column density in H.

(b) Following Spitzer (1978), a standard curve of growth was calculated for velocity parameters $b = 20,60,100,140 \text{ km s}^{-1}$ (Figs. 8a-d). The predicted equivalent widths of Ly α , CIV, NV, and (OVI) were then compared with those derived from the analysis of the HST spectrum.

We find that at the ROSAT low-state (which is close to the state of the source at the time of the ASCA observations), and for b about 60 km s^{-1} , there is a rough match between the Ly α and CIV absorption lines produced by the warm absorber and the observed lines at $z = 0.098$ and $z = 0.090$ (models c-e). The NV absorption line from the warm absorber is, however, always weaker than observed (N is too highly ionized in the models). Including an additional EUV bump will further increase the level of ionization, thus not changing the above conclusions. The different models differ most strongly in OVI, so this may be the most restrictive line, but it falls just outside the HST range.

In conclusion, we find no single-phase medium which can produce both the UV and the X-ray absorption lines.

(c) In the case of the best fit to the ASCA data i.e. the model with Fe overabundant by a factor of ~ 22 over solar, the degree of ionization is not known but it is likely to be too high for the production of the CIII* absorption line. Thus, in this case also, the UV and X-ray absorbers are very probably in different gaseous phases.

5.2. Emission lines from the Warm Absorber

Tab. 5 gives the intensity of the strongest lines emitted by the absorber within the wavelength range of the HST spectra and in the optical range. The calculations were performed with a density of $\log n_{WA} = 9.5$. The line NeVIII λ 774 was added to the list because of recent reports of its detection in high- z quasars (Hamann et al. 1997). Table 5 is meant to provide an order of magnitude estimate of which lines may be important/detectable in the future. The actual strength of the lines depends on the covering factor of the warm absorber; total coverage was assumed for the values in Table 5.

5.3. Relation between the X-ray and the UV absorber

In the recent years it has been realized that gas outflow is ubiquitous in AGN. It occurs under different gas phases: broad emission line gas (the most highly ionized lines are the most blueshifted) and UV/optical absorption lines (always observed at rest or blueshifted). It is likely that the X-ray absorption features also, originate in outflowing gas at velocities comparable with or higher than those of the UV emission/absorption gas - this cannot presently be ascertained because of the insufficient energy resolution of the X-ray instruments. [This is not counting here the extraordinary blueshift of the X-ray absorbing gas if the 1 keV features are blueshifted OVII or OVII edges].

The question as to whether UV absorption lines and X-ray absorption lines/edges tend to be present together or separately in AGN has been addressed by Ulrich (1988) and more recently by a number of authors (e.g. Schartel et al. 1997, Crenshaw 1997, Mathur 1997, Shields & Hamann 1997, Kriss et al 1996).

In some AGN, the data appear consistent with a single-phase, photoionized plasma producing the UV absorption and the OVII and OVIII edges (NGC 3783 Shields & Hamann 1997; 3C212, 3C351 and NGC 5548 Mathur 1997). In contrast, in other AGN, the properties of the UV and the X-ray absorbers imply the presence of multiphase media (NGC 3516 Kriss et al 1996; MCG-6-3-15 Otani et al 1996). The present analysis indicates that PG1404+226 is another such case of multiphase absorbing medium (but the non-simultaneity of the observations has to be kept in mind).

With the detection of X-ray and UV absorption in PG1404+226 the statistical association between the presence of UV absorption lines and X-ray absorption edges becomes stronger (Ulrich 1988, Mathur Wilkes & Elvis

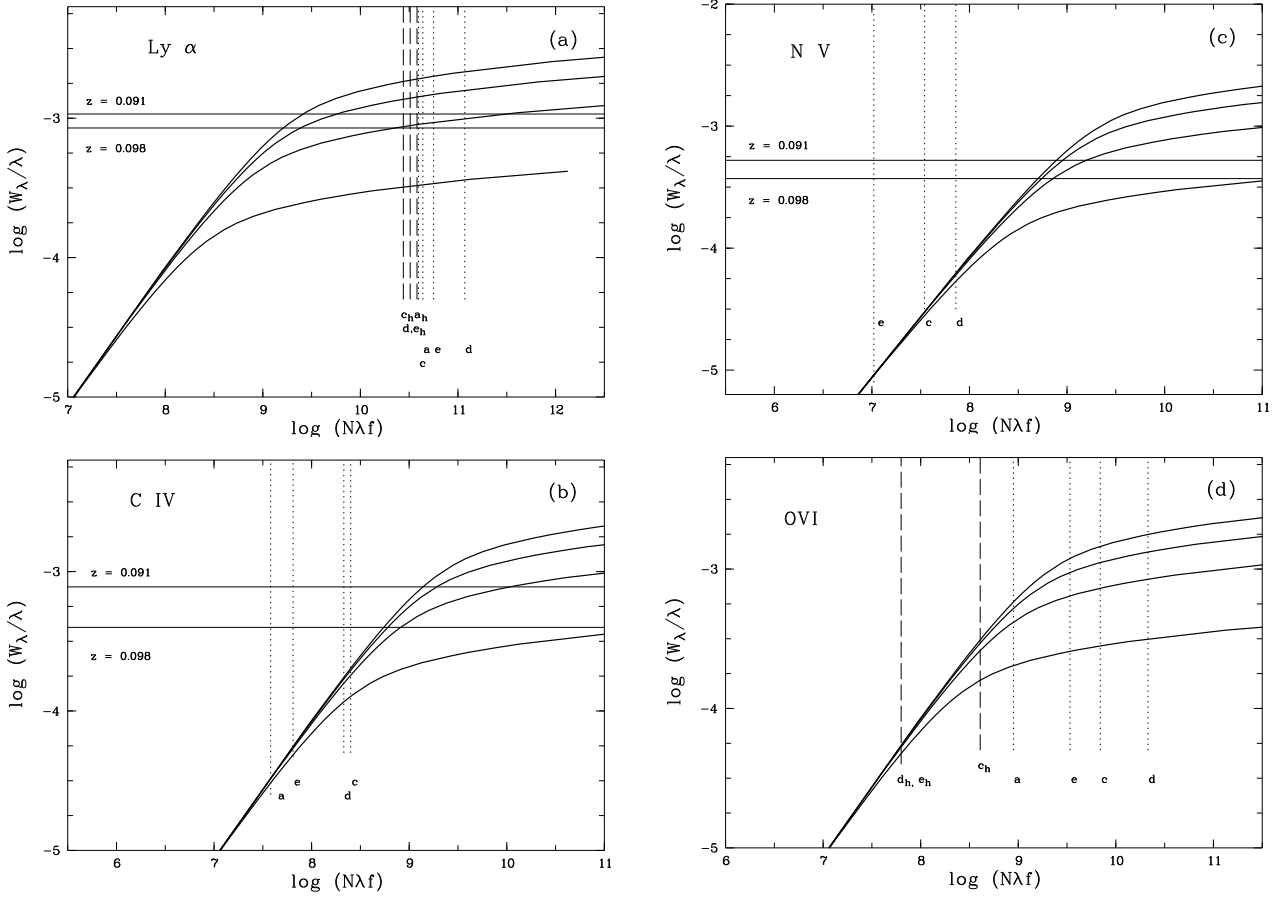


Fig. 8. Comparison of HST UV absorption measurements with the UV absorption in Ly α , CIV, NV, and OVI predicted by a warm absorber. Thick lines: curves of growth calculated for velocity parameters $b = 20, 60, 100, 140$ km s $^{-1}$ from bottom to top (for definition of standard quantities; see Spitzer 1978). Horizontal lines: Observed EW of the two UV absorption systems. Vertical lines: predictions from the WA models (a) - (e) as defined in Section 2.2. Predictions for the high-state data are printed as dashed lines and the letters have an index h added, whereas predictions for the low-state are shown as dotted lines and letters without index. Definition of axis: W_λ = equivalent width, λ = wavelength, N = column density in the relevant ion, f = oscillator strength.

Table 5. Emission lines predicted by the warm absorber models. To judge the detectability of these lines, their luminosity was scaled to the one observed in Ly α and assuming 100% covering of the warm material. Line-ratios less than 0.01 are not listed. The emission lines given below are: NeVIII 774, OVI 1035, FeXXI 1354, and FeXIV 5303. HS and LS refer to ROSAT high-state and low-state, respectively.

state	$\log U$	$\log N_w$	$I/I_{Ly\alpha,obs}$				model
			NeVIII	OVI	FeXXI	FeXIV	
HS/LS	0.7/0.3	23.3/22.9	1.6	0.1	1.7	-	(c): Ne = 4×solar abundance
HS/LS	0.7/0.5	23.5/23.4	1.3	0.2	2.5	0.01	O = 0.4×solar abundance
HS/LS	0.6/0.4	23.1/23.1	0.1	0.05	1.2	-	(e): additional 0.1 keV soft excess

1998). The two absorbers could be two different gaseous phases, partaking in the same outflow but differing by their physical conditions, velocity and radial distance to the central black hole.

6. Conclusions

The main results of our analysis can be summarized as follows:

1) The X-ray spectrum of PG 1404+226 is variable by a factor 4 in $\sim 3 \times 10^4$ s and is characterized by a strong soft excess below 2 keV whose luminosity ($L_{Soft} \sim 7 \times 10^{43}$

erg s⁻¹ in the 0.4–2.0 keV energy range) is about a factor 3 greater than the 2–10 keV luminosity (L_{Hard}).

The soft excess emission can be described with a high temperature optically thick blackbody ($kT \sim 140$ eV). Optically thin models are ruled out combining the observed luminosity with the dimension of the region derived from the variability timescale.

2) The residuals around 1 keV can be best described by an absorption edge at $E = 1.07 \pm 0.03$ keV, *not* consistent with being caused by highly ionized oxygen at rest in the quasar frame. A possible explanation could be either in terms of iron overabundance, as suggested by the warm absorber fits and the extremely high EW of the iron K α line, or by resonant absorption in a turbulent gas. The interpretation of a blueshifted Oxygen edge in a relativistically outflowing gas is less likely and not supported by the optical–UV data. X–ray observations of NLS1 at high spectral resolution with XMM and *Chandra* will allow to clarify the origin of the 1 keV absorption detected in PG 1404+226 and 3 other NLS1.

3) Two systems of absorption lines separated by ~ 1900 km s⁻¹ are identified in the FOS/HST spectra in the lines of Ly α , C IV and N V. One system is located to the red of the emission line peaks. Considering that in most radio quiet QSOs the highly ionized emission lines are blueshifted (as part of an outflow from the face of the accretion disk turned toward us) we argue that this absorption system is nearly at rest in the AGN frame. Its properties are consistent with this absorber being produced in the halo of the host galaxy or a companion. As for the system blueshifted by ~ 1900 km s⁻¹, the very probable detection of CIII* λ 1175 (which has been seen in absorption only in NGC 4151 - Bromage et al. 1985, Kriss et al. 1992) indicates that this system is intrinsic to the quasar.

4) With the detection of X-ray and UV absorption in PG1404+226 the statistical association between the presence of UV absorption lines and X-ray absorption edges first suggested by Ulrich (1988) is becoming clearer (Mathur Wilkes & Elvis 1998). We may be seeing two different absorbers with different physical conditions and locations but both being parts of a grand design outflow. The differences observed among absorption features in various AGN are likely to result from intrinsic differences in the properties of the gaseous outflows, from differences in the aspect angles and from the shape of the X–ray spectrum.

Acknowledgements. We thank Gary Ferland for providing Cloudy. AC acknowledges partial support by the Italian Space Agency (ASI) under the contract ASI-ARS-96-70 and by the Italian Ministry for University and Research (MURST) under grant Cofin98-02-32. St. K. acknowledges support from the Verbundforschung under grant No. 50 OR 93065, and P.C. acknowledges support from NASA through contract NAS5-26670.

References

- Boller T., Brandt W.N., Fink H., 1996, A&A, 305, 53
 Boroson T.A., Green R.F., 1992, ApJS, 80, 109
 Brandt W.N., Fabian A.C., Nandra K., Reynolds C. S., Brinkmann W., 1994, MNRAS 271, 958
 Brandt W.N., Mathur S., Elvis M., 1997, MNRAS 285, L25
 Bromage G.E., Boksenberd A., Clavel J., et al. 1985, MNRAS, 215, 1
 Comastri A., Setti G., Zamorani G., et al 1992, ApJ 384, 62
 Comastri A., Molendi S., Ulrich M.-H., 1997, (CMU97) in *X-Ray Imaging and Spectroscopy of Cosmic Hot Plasmas*, F. Makino, K. Mitsuda (eds), 279
 Comastri A., Fiore F., Guainazzi M., et al 1998, A & A 333, 31
 Comastri A., Brandt, W. N., Leighly, K. M., et al. 1998, Proceedings of the Conference *The Active X-Ray Sky, Results from BeppoSAX and RXTE*, Scarsi L. et al eds Nuclear Physics B Suppl. 69/1 page 523
 Corbin M.R., 1995, ApJ, 447, 496
 Crenshaw D.M., 1997 in *Mass Ejection from Active Galactic Nuclei*, Arav N., Shlosman I., Weymann R.J., eds, ASP Conf. Series, Vol., 128, 121
 Czerny B., Witt H. J., Zycki P. T., 1996 INTEGRAL Workshop, *The Transparent Universe*, St. Malo, September 1996
 Done C., Mulchaey J. S., Mushotzky R. F., Arnaud K. A., 1992, ApJ 395, 275
 Elvis M., Lockman F.J., Wilkes B.J., 1989, AJ, 97, 777
 Ferland G.J. 1993, University of Kentucky, Physics Department, Internal Report
 Fink H., Walter R., Schartel N., Engels D., 1997, A&A, 317, 25
 Fiore F., Matt G., Cappi M., et al 1998, MNRAS, 298, 103
 Grupe D., 1996, PhD Thesis (University of Göttingen)
 Haardt F., Maraschi L., 1993, ApJ, 413,507
 Hamann F. Ferland G.J. 1993, ApJ, 418, 11
 Hamann F., Cohen R.D., Shields J.C., Burbidge E.M., Junkkarinen V., Crenshaw D.M., 1997, ApJ, 496, 761
 Hayashida K., 1997 in *Emission Lines in Active Galaxies: New Methods and Techniques* Peterson B.M., Cheng F.-Z., Wilson A.S., eds, ASP Conference Series Vol. 113, 40 Vol. 113, 40
 Komossa S., Fink H., 1997 A&A, 322, 719
 Kriss G.A., Davidsen A. F., Blair W. P., et al., 1992, APJ, 392, 485
 Kriss G.A., Espey B. R., Krolik J. H., et al 1996, ApJ, 467, 622
 Krolik J.H., Kriss G.A., 1995, ApJ, 447, 512
 Laor A., Fiore, F., Elvis, M., et al 1994, ApJ 435, 611
 Laor A., Bahcall J. N., Jannuzi B. T., et al 1995, ApJS 99, 1
 Laor A., Januzzi B.T., Green R.F., Boroson T.A., 1997 in *Emission Lines in Active Galaxies: New Methods and Techniques* Peterson B.M., Cheng F.-Z., Wilson A.S., eds, ASP Conference Series Vol. 113, 116
 Leighly K.M., Mushotzky R.F., Nandra K., Forster K., 1997, ApJ, 489, L25
 Marshall F. E., Netzer H., Arnaud K. A., 1993, ApJ, 405, 168
 Mathur S., 1997 in *Mass Ejection from Active Galactic Nuclei* ASP Conf. Series, Vol., 128, 161 Arav N., Shlosman I., Weymann R.J., eds ASP Conf. Series, Vol., 128, 161
 Mathur S., Wilkes B., Elvis M., 1998, ApJ, 503, L23
 Netzer, H., Turner T. J., 1997 ApJ, 488, 694

- Nicastro F., Fiore F., Perola G. C., Elvis M., 1999a, ApJ 512, 184
- Nicastro F., Fiore F., Matt G., 1999b, ApJ 517, 108
- Osterbrock D.E., Pogge R., 1985, ApJ., 297, 166
- Otani C., Kii T., Miya K., 1996 in *Intern. Conf. on X-Ray Astron. and Astrophys., MPE Report, 263* Zimmermann H.-U., Trümper J.E., Yorke H., eds., 491
- Pounds K.A., Done C., Osborne J.P., 1995, MNRAS, 277, L5
- Reynolds C.S., Fabian A.C., 1995, MNRAS, 273, 1167
- Reynolds C.S., Fabian A.C., Inoue H., 1995, MNRAS, 276, 1311
- Reynolds C.S., 1997, MNRAS 286, 513
- Schartel N., Komossa S., Brinkmann W., Fink H.H., Trümper J., Wamsteker W., 1997, A&A 320, 421
- Shields J.C., Hamann F., 1997, ApJ, 481, 752
- Shuder J.M., Osterbrock D.E., 1981, ApJ., 250, 55
- Spitzer L., 1978, *Physical Processes in the Interstellar Medium*. John Wiley Sons, New York
- Sulentic J.W., Marziani P., Zwitter T., Calvani M., 1995, ApJ, 438, L1
- Tanaka Y., Inoue H., Holt S.S., 1994, PASJ 46, L37
- Ulrich M.-H., 1988, MNRAS, 230, 121
- Ulrich M.-H., Molendi S., 1996, ApJ, 457, 77 (UM96)
- Van Groningen E. 1987, A&A, 186, 103
- Zdziarski A., Ghisellini, G., George, I.M. et al. 1990, ApJ, 363, L1